Initial-Stage Growth Controlled Crystal Orientations in Nanoconfined Lamellae of a Self-Assembled Crystalline−Amorphous Diblock Copolymer

Lei Zhu, Bret H. Calhoun, Qing Ge, Roderic P. Quirk, and Stephen Z. D. Cheng*

Maurice Morton Institute and Department of Polymer Science, The University of Akron, Akron, Ohio 44325-3909

Edwin L. Thomas

Department of Materials Science and Engineering, Massachusetts Institute and Technology, Cambridge, Massachusetts 02139

Benjamin S. Hsiao, Fengji Yeh, and Lizhi Liu

Department of Chemistry, The State University of New York at Stony Brook, Stony Brook, New York 11794-3400

Bernard Lotz

Institute Charles Sadron, 6 Rue Boussingault, Strasbourg 67083, France

Received October 31, 2000; Revised Manuscript Received December 12, 2000

ABSTRACT: Crystallization temperature (T_c)-dependent crystal orientations within nanoconfined lamellae have been studied in a self-assembled poly(ethylene oxide)-*block*-polystyrene (PEO-*b*-PS) diblock copolymer. The copolymer possesses number-average molecular weights of $\bar{M}_n^{PEO} = 8.7$K and $\bar{M}_n^{PS} = 9.2$K, and it forms a microphase-separated lamellar structure in the melt. It has been found that the PEO crystal (the *c* axis) orientations are determined by only varying the T_c.[1] Based on real-time simultaneous two-dimensional (2D) small-angle X-ray scattering (SAXS) and wide-angle X-ray scattering (WAXS) experiments, the formation of crystal orientation is found in an early stage of PEO crystallization confined between the PS lamellae. To understand whether the crystal orientation is determined during the primary nucleation or crystal growth step, specifically designed self-seeded crystallization experiments are carried out using 2D SAXS and WAXS techniques. Experimental results suggest that primary nuclei (self-seeds) do not possess specific orientation with respect to the PS lamellar surface normal, disregarding the history of crystal orientation in the samples generated before the self-seeding process. It is found that the initial stage of crystal growth determines the final crystal orientation in the nanoconfined lamellae. Studies of the correlation lengths (apparent crystallite sizes) along both [120] directions of the PEO crystals with various crystal orientations indicate that the PEO crystals formed in nanoconfined lamellae undergo a change from a one-dimensional to a two-dimensional growth with increasing T_c.

Introduction

Polymers in confined environments are of great scientific interest. During the past decade, polymer phase transformations, such as glass transition, liquid crystal formation, and crystallization, in confined geometries have received intensive investigation. Porous inorganic materials, such as clay, ceramic, silicate gel, molecular sieve, and zeolite, are often used as templates to construct nanoconfined environments.[2−5] Other than these inorganic materials, it is well documented that various ordered phase morphologies, such as lamellae, double gyroid, cylinders, and spheres, have been found for diblock copolymers on a length scale of a few tens of nanometers as a consequence of microphase separation of the dissimilar components below the order−disorder transition temperature (T_{ODT}).[6] Therefore, a convenient and effective way to construct well-defined and uniformly oriented nanoenvironments is to use diblock copolymers as templates. For example, confined polymer crystallization can be studied using microphase-separated crystalline−amorphous diblock copolymers.[1,7−10] To ensure a "solid" confinement environment, the amorphous blocks need to possess a glass transition temperature (T_g^a) which is higher than the melting temperature of the crystals (T_m^c) formed by the crystallizable blocks, namely, $T_{ODT} > T_g^a > T_m^c$.[10]

Among various phase morphologies of block copolymers, the lamellar morphology, which is one-dimensionally (1D) confined, constructs the simplest confinement geometry. Over the past four decades, the crystal orientation (usually represented by the *c* axis orientation) in confined lamellae has been studied using lamellar-forming diblock copolymers. Various crystal orientations have been observed experimentally for different block copolymers. For some poly(ethylene oxide) (PEO)-containing diblock copolmyers, a homeotropic crystal orientation with respect to the lamellar surface has been found, meaning the chain direction (the *c* axis) in the PEO crystals is parallel to the lamellar surface normal ($\hat{n}$).[11−15] On the other hand, for some shear-aligned polyethylene (PE)-containing diblock copolymers, a homogeneous crystal orientation was observed, where the *c* axis orientation in PE crystals is

* To whom correspondence should be addressed. E-mail: cheng@polymer.uakron.edu.

10.1021/ma001882p CCC: $20.00
Published on Web 01/27/2001

Scheme 1. Schematic Representation of Shearing Geometry for the PEO-*b*-PS Sample

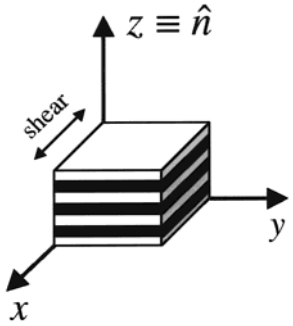

perpendicular to $\hat{n}$.[16−20] Recently, tilted crystal orientations with respect to $\hat{n}$ have also been proposed on the basis of experimental observations.[21,22] Different crystal orientations in the confined lamellae are speculated to be dependent upon various types of block copolymers and different block lengths.

Most recently, a lamellar-forming PEO-*b*-PS (8.7K−9.2K) diblock copolymer was studied. Differential scanning calorimetry (DSC) results show that this diblock copolymer possesses a glass transition temperature of the PS blocks (T_g^{PS}) of 62 °C and a melting temperature of the PEO blocks (T_m^{PEO}) of ∼51 °C (for crystallization temperature, T_c < 40 °C).[9] Based on small-angle X-ray scattering (SAXS) and transmission electron microscopy (TEM) observations, the overall long period, the thicknesses of the PS layer, and the PEO layer are 18.7, 9.9, and 8.8 nm, respectively.[9] Thus, between two glassy PS layers the PEO blocks crystallize in a 1D confined lamellar space of 8.8 nm. The T_{ODT} is determined to be 160 °C by temperature-dependent 1D SAXS. The confined crystallization process of the PEO blocks between the glassy PS layers has also been followed by time-resolved simultaneous 1D SAXS and wide-angle X-ray scattering (WAXS) experiments.[9]

T_c-dependent PEO crystal orientations in confined lamellae of this diblock copolymer have recently been reported.[1] After shearing, the lamellar morphology is macroscopically aligned parallel to the *xy* plane, and $\hat{n}$ is parallel to the *z* direction (see Scheme 1). Four T_c regions have been observed for different crystal orientations: (1) T_c < −50 °C, (2) −50 °C ≤ T_c ≤ −10 °C, (3) −5 °C ≤ T_c ≤ 30 °C, and (4) T_c ≥ 35 °C. For T_c < −50 °C (e.g., quickly quenched into liquid nitrogen from the melt at 70 °C), the PEO crystals are randomly oriented. Between −50 °C ≤ T_c ≤ −10 °C, the *c* axis of the PEO crystals orients perpendicular to $\hat{n}$ (homogeneous orientation). When −5 °C ≤ T_c ≤ 30 °C, the *c* axis of the PEO crystals is inclined with respect to $\hat{n}$. The tilt angle with respect to the *xy* plane increases with increasing the T_c. Finally, for T_c ≥ 35 °C, the *c* axis of the PEO crystals is parallel to $\hat{n}$ (homeotropic orientation).[1]

In this publication, the focus is to determine in which crystallization step the specific crystal orientation forms. Simultaneous time-resolved two-dimensional (2D) SAXS and WAXS experiments show that the crystal orientation is formed in an early stage of crystallization. To identify whether the primary nucleation or the crystal growth in this early stage of crystallization determines the final crystal orientation in the 1D nanoconfined lamellae, specific self-seeded crystallizations are designed. The (120) correlation lengths along two perpendicular [120] directions of the PEO crystals are also analyzed for various crystal orientations in the confined lamellae. The results suggest an interesting and important observation of the T_c-dependent crystal growth dimensionality within the nanoconfined environment.

Experimental Section

Materials and Sample Preparation. The PEO-*b*-PS diblock copolymer was synthesized via sequential anionic block copolymerization of styrene and ethylene oxide. Detailed synthesis procedures can be found elsewhere.[23,24] The PS precursor was characterized by size exclusion chromatography (SEC) using polystyrene standards and had an $\bar{M}_n$ of 9.2K and a polydispersity of 1.02. The $\bar{M}_n$ of the PEO blocks was determined by proton nuclear magnetic resonance (^{1}H NMR) to be 8.7K, and the polydispersity of 1.04 in the final diblock copolymer was determined by SEC using a universal calibration. The volume fraction of PEO blocks is thus 0.473 in the melt at 60 °C (the densities of amorphous PEO and PS are 1.092 and 1.035 g/cm^3).[9]

All the samples were prepared by a consistent method with identical thermal history to ensure consistency of the phase morphology. The samples were cast from a 5% (w/v) toluene solution, and the solvent was evaporated slowly in dry nitrogen at 50 °C to prevent interference of PEO block crystallization. Residual solvent was further removed under vacuum at 50 °C for 1 day, and the sample was then annealed at 95 °C (which is lower than the T_{ODT} and higher than the T_g^{PS} and T_m^{PEO}) for 12 h to allow the development of the equilibrium phase morphology. To study the crystal orientation in this copolymer, the phase-separated samples were subjected to large-amplitude oscillating shear under a dry argon atmosphere at 110 °C to achieve uniform, parallel alignment of the lamellar phase morphology. The shear geometry has been shown in Scheme 1. The shear direction is along the *x* direction, and the shear gradient is along the *z* direction. The shear frequency was 0.5 Hz, and the shear amplitude was 150%. The shear-aligned samples were further annealed at 95 °C for another 12 h in a vacuum to eliminate any residual stresses and perfect the lamellar phase morphology. The sample size was around 1.0 × 1.0 × 0.2 mm^3.

Equipment and Experiments. Simultaneous two-dimensional (2D) SAXS and WAXS experiments were carried out at the synchrotron X-ray beamline X27C at the National Synchrotron Light Source in Brookhaven National Laboratory. The wavelength of the X-ray beam was 0.1307 nm. The zero pixel of the 2D SAXS pattern was calibrated using silver behenate, with the first-order scattering vector q ($q = 4\pi \sin\theta/\lambda$, where λ is the wavelength and 2θ the scattering angle) being 1.076 nm^{-1}. 2D WAXS were calibrated using α-Al_2O_3 with known crystal reflections, and air scattering was subtracted. Conventional 2D WAXS experiments were conducted on a Rigaku 18 kW rotating anode generator equipped with an image plate as the detector. This equipment was calibrated using silicon powder ($2\theta = 28.4°$) under Cu Kα radiation. The air scattering was also subtracted. The same samples were used in both synchrotron and conventional WAXS experiments. Longitudinal and transverse profiles for the 2D WAXS patterns were obtained via scans along vertical and horizontal directions. Isothermal crystallization measurements were carried out on a customized two-chamber hot stage. The isothermal crystallization temperature (T_c) was controlled to within ±0.1 °C. The samples were preheated to 70 °C in the melting chamber for 3 min and then quenched (switched) to the second chamber with preset temperatures for isothermal crystallization. The WAXS crystallinity of the PEO blocks was determined by normalizing the crystallinity to the PEO weight fraction in the integrated 2D WAXS patterns.

To analyze the correlation lengths (apparent crystallite sizes), the Scherrer equation was used:

$$D_{hkl} = \frac{K\lambda}{\beta_{hkl}\cos\theta} \tag{1}$$

where D_{hkl} is the mean crystallite size along the [*hkl*] direction, and K is the shape factor (the Scherrer constant, and a value

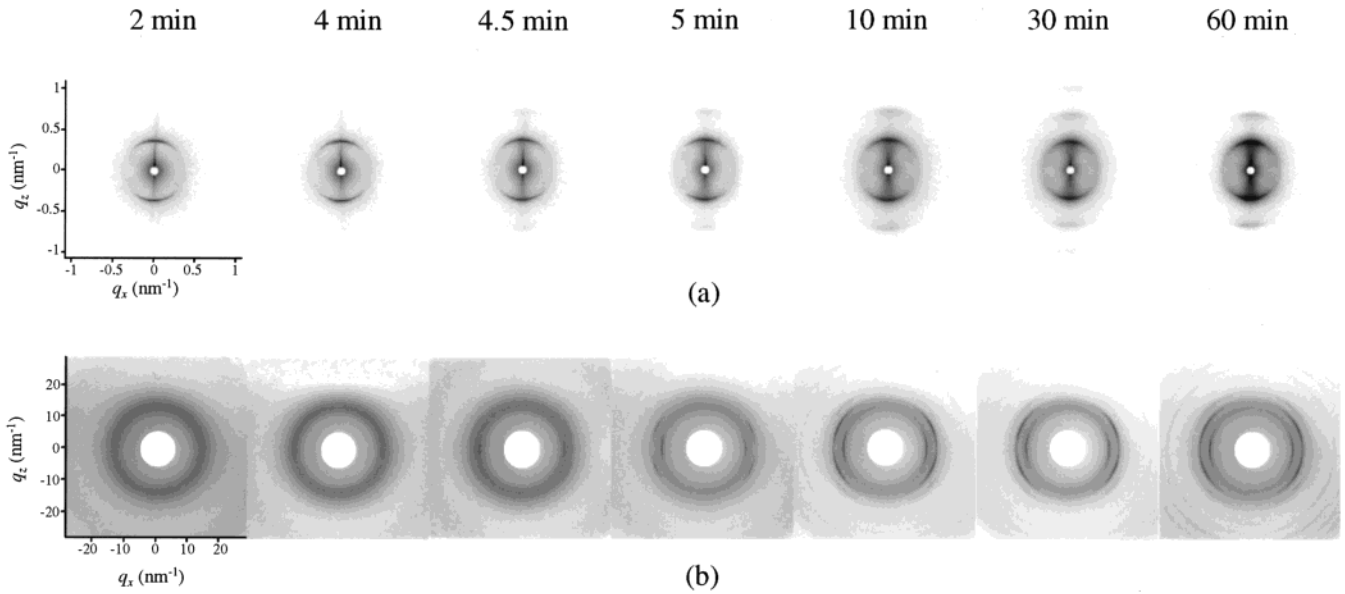

Figure 1. Sets of SAXS (a) and WAXS (b) patterns for the shear-aligned PEO-*b*-PS isothermally crystallized at 36 °C for different times. Both SAXS and WAXS intensities are in logarithmic scales.

of 0.94 is used in this case[25]). β_{hkl} is the pure line breadth, and θ is the half-scattering angle. Usually, β_{hkl} was taken as the half-width of the (hkl) diffraction. Assuming that the diffraction peak shape obeyed a Gaussian function, Warren's correction can be used to correct instrument broadening:[25]

$$\frac{\beta_{hkl}}{B_{hkl}} = \sqrt{1 - \frac{b^2}{B_{hkl}^2}} \qquad (2)$$

where B_{hkl} is the experimentally observed half-width at half-maximum (hwhm) of the diffraction peak, and b is the hwhm of a standard specimen diffraction. To ensure a good calibration, the mean crystallite size of the standard specimen should be over 60 nm. A quartz line at 60.0° was taken for standard b. The broadening factor caused by Cu Kα_1 and Kα_2 lines was also taken into account in the calculation.

Isothermal crystallization experiments were conducted using an Instec LN2-P2 hot stage equipped with a liquid nitrogen cooling system. The isothermal T_c was controlled to within ±0.1 °C. The shear-aligned samples were preheated to 70 °C for 3 min on another hot stage and then quickly switched to the hot stage at a preset T_c for crystallization.

Transmission electron microscopy (TEM, JEOL, 1200 EX II) experiments were carried out at an accelerating voltage of 120 kV. Thin slices for TEM experiments were obtained using a Reichert Ultracut S (Leica) ultra-cryomicrotome to section the shear-aligned samples parallel to the z direction (see Scheme 1). The sample was stained under RuO_4 vapor for 20 min at room temperature.[26]

Results and Discussion

Formation of Crystal Orientation during Isothermal Crystallization. Time-resolved simultaneous 2D WAXS and SAXS experiments are conducted to monitor the crystal formation within the confined lamellae. Since the crystallization rate is very fast when T_c < 25 °C (crystallization time for developing half of the overall crystallinity, $t_c^{1/2}$, is less than 2 min), only the crystallization kinetics at T_c's > 25 °C are studied. Figure 1a,b shows the time-resolved simultaneous 2D SAXS and WAXS along the y direction at T_c = 36 °C (note that the X-ray diffraction patterns along both the x and y directions are identical). The azimuthal integrated WAXS curves for the 2D WAXS at different crystallization times (t_c) are shown in Figure 2. At t_c =

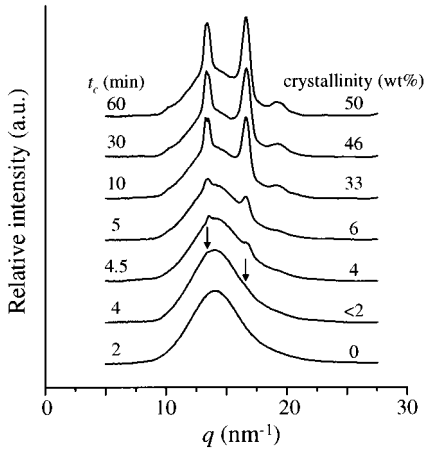

Figure 2. Azimuthal integrated WAXS patterns (from Figure 1b) for the sample crystallized at 36 °C.

2 min, an amorphous halo is observed in the 2D WAXS pattern (see Figures 1b and 2), while the 2D SAXS shows oriented lamellar phase morphology with $\hat{n}||z$ (Figure 1a). At t_c = 4 min, very weak (120) reflections and the overlapped ($\bar{1}32$), (032), (112), ($\bar{2}12$), ($\bar{1}24$), ($\bar{2}04$), and (004) reflections can be observed in the azimuthal integrated WAXS curve (see arrows in Figure 2), although they are weak in the 2D WAXS pattern in Figure 1b. At this time, the crystallinity is estimated to be < 2 wt %. At t_c = 4.5 min, the (120) reflections and the overlapped reflections become clear, and the crystallinity is estimated to be around 4 wt % (Figure 2). It is evident that even at this early crystallization stage the homeotropic crystal orientation has formed, judging by the fact that (120) reflections are located in the xy plane and the overlapped ($\bar{1}32$), (032), (112), ($\bar{2}12$), ($\bar{1}24$), ($\bar{2}04$), and (004) reflections are oriented at 23° away from the xy plane.[1] With further increasing the t_c, the crystallinity gradually increases in the WAXS (Figures 1b and 2), and higher index reflections also gradually develop in the 2D SAXS (Figure 1a). The crystal orientation and the orientation factor do not change during the rest of the isothermal crystallization process. Therefore, the homeotropic crystal orientation is found in an early stage of crystallization with a lower

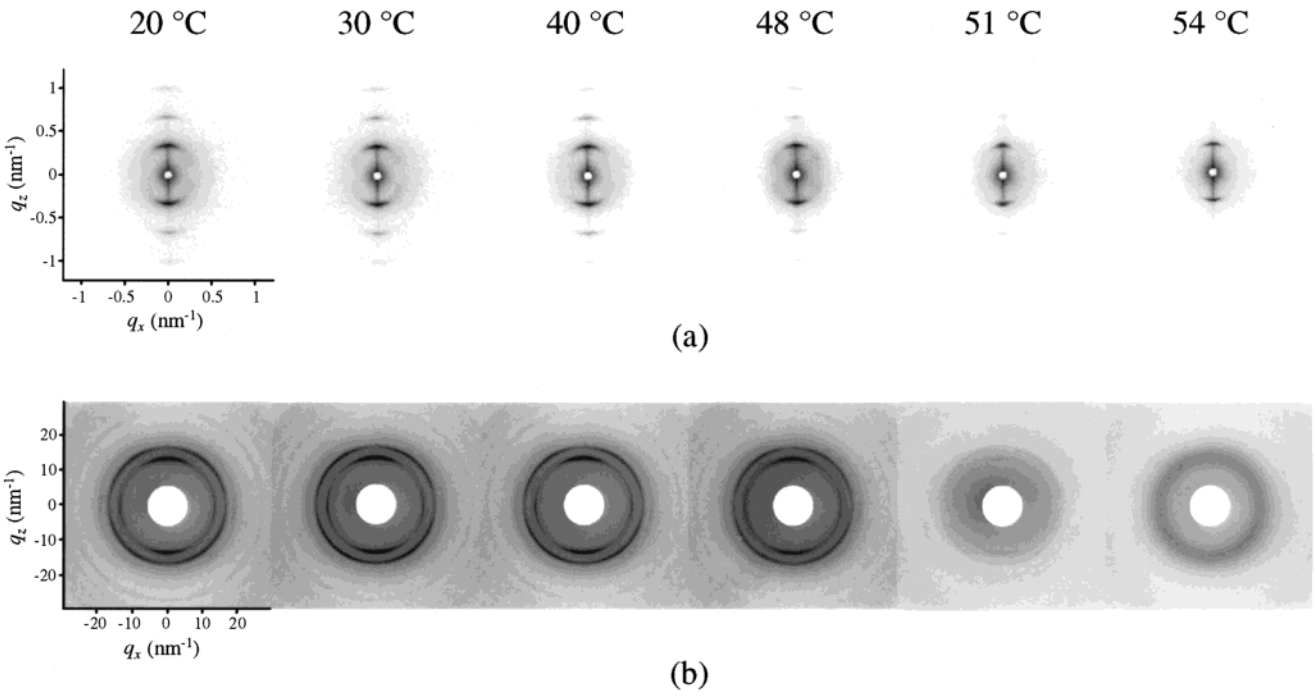

Figure 3. Set of time-resolved 2D SAXS (a) and WAXS (b) patterns for the shear-aligned PEO-*b*-PS during heating at 1 °C/min after being isothermally crystallized at −20 °C. Both SAXS and WAXS intensities are in logarithmic scales.

limit of crystallinity ∼5 wt %. All subsequent crystallization process is merely to increase crystallinity without changing of the crystal orientation in the system.

Understanding the Determining Factors for the Crystal Orientation. The early stage crystallization includes two important steps: primary nucleation and initial stage of crystal growth (surface nucleation). To recognize which step determines the crystal orientation, specific self-seeding experiments are designed (slightly modified from the procedures previously described[27,28]). The idea is to use self-seeds as primary nuclei, and thus the primary nucleation step can be separated from the subsequent crystal growth. A sample having a homogeneous crystal orientation (crystallized at $T_c = -20$ °C) is first heated to a temperature where very few percent crystallinity is remained to serve as self-seeds. Then, it is quenched to a preset T_c (at $T_c \geq 35$ °C) and isothermally crystallized there. Note that the homeotropic crystal orientation forms at this T_c in non-self-seeded crystallization. If the final crystal orientation is identical to that in the first isothermal crystallization at $T_c = -20$ °C (i.e., the homogeneous orientation), then the orientation of the primary nucleation determines the final crystal orientation. If the final crystal orientation transforms to the homeotropic crystal orientation after self-seeded crystallization, on the other hand, the primary nucleation is not a determining step for the crystal orientation. Instead, the determining step is the initial stage of crystal growth.

To ensure consistent crystal orientation during the heating process of the self-seeding experiment, the heating process of a shear-aligned PEO-*b*-PS diblock copolymer sample with a homogeneous crystal orientation ($T_c = -20$ °C) is monitored by time-resolved simultaneous 2D SAXS and WAXS, as shown in Figures 3a,b. The heating rate is kept at 1 °C/min. Upon heating, the crystallinity decreases starting at 40 °C due to the PEO crystal melting. The homogeneous crystal orientation does not change until the sample melts. In the self-seeding experiment, we choose the self-seeding temperature (T_s) at 54 °C, because from the DSC result, the remaining crystallinity at 54.0 °C is less than 1 wt %. After the T_s is reached, the sample is directly quenched to a preset $T_c = 40$ °C for isothermal crystallization. Note that the PEO crystallization kinetics is very slow at $T_c = 40$ °C if the sample is directly quenched from the melt (70 °C). In other words, the formation of primary nuclei from the PEO melt is difficult at 40 °C. The crystallization kinetics of the self-seeded crystallization and the non-self-seeded crystallization at 40 °C are compared in Figure 4. In this figure, the $t_c^{1/2}$ for the self-seeded crystallization is 10 min, while it is 600 min for non-self-seeded crystallization. The self-seeded PEO-*b*-PS sample almost does not need induction time for crystallization, because the self-seeds provide surface sites for crystal growth. However, the non-self-seeded sample needs 100 min of induction time for the PEO block crystallization. This result confirms that the self-

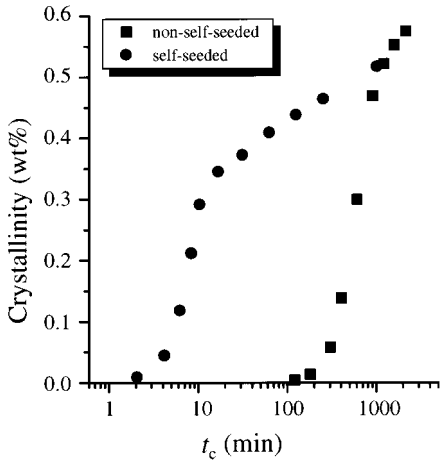

Figure 4. Isothermal crystallization kinetics at 40 °C for both the self-seeded and non-self-seeded PEO-*b*-PS samples.

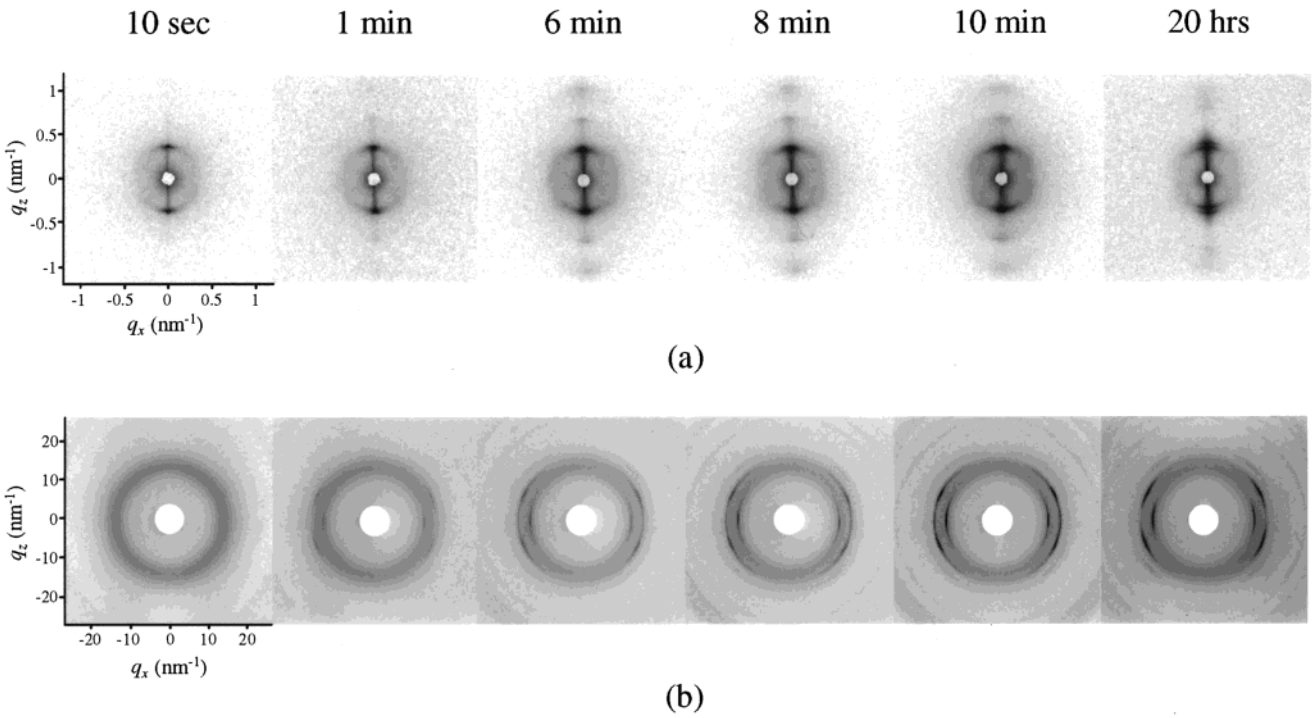

Figure 5. Set of time-resolved 2D SAXS (a) and WAXS (b) patterns for the self-seeded PEO-*b*-PS crystallized at 40 °C for different times. The sample was originally crystallized at −20 °C. Both SAXS and WAXS intensities are in logarithmic scales.

seeds exclusively serve as primary nuclei during the self-seeded crystallization. It should also be noted that the t_c to enter the secondary crystallization (the change in the slope in Figure 4) is earlier in the self-seeded sample than that of the non-self-seeded sample. This may indicate that the impingement of the crystals takes place earlier in the self-seeded sample due to a higher primary nucleation density after the self-seeding process.

The self-seeded crystallization at 40 °C is monitored by time-resolved simultaneous 2D SAXS and WAXS experiments along the *y* direction (Figures 5a,b). The azimuthal integrated SAXS and WAXS curves are shown in parts a and b of Figure 6, respectively. At t_c = 10 s, an amorphous halo can be observed in the 2D WAXS, while the 2D SAXS shows ordered lamellar scattering on the *z* direction. At t_c = 1 min, the (120) reflections appear in the *xy* plane, and the overlapped ($\bar{1}$32), (032), (112), ($\bar{2}$12), (124), ($\bar{2}$04), and (004) reflections are oriented at 23° away from the *xy* plane in the 2D WAXS pattern, indicating a homeotropic crystal orientation within the nanoconfined lamellae. In the azimuthal integrated SAXS in Figure 6a the first-order scattering peak becomes stronger and slightly broader than that in the melt. This is attributed to the crystallization of the PEO blocks.[9] The overall crystallinity is about 5 wt %, as estimated from the WAXS result in Figure 6b. With further increasing the t_c, the PEO crystallinity increases substantially. These results clearly illustrate that the crystal orientation within the confined lamellae transforms to the homeotropic orientation after self-seeding and subsequent isothermal crystallization at 40 °C. The self-seeds, which serve as primary nuclei in the self-seeded crystallization, do not have memory of the original orientation in the homogeneous crystals formed at T_c = −20 °C. It is speculated that the self-seeds (primary nuclei) are too small in size to "*feel*" the 1D confined lamellae of 8.8 nm, and they can easily change their orientation within the nanolamellae.

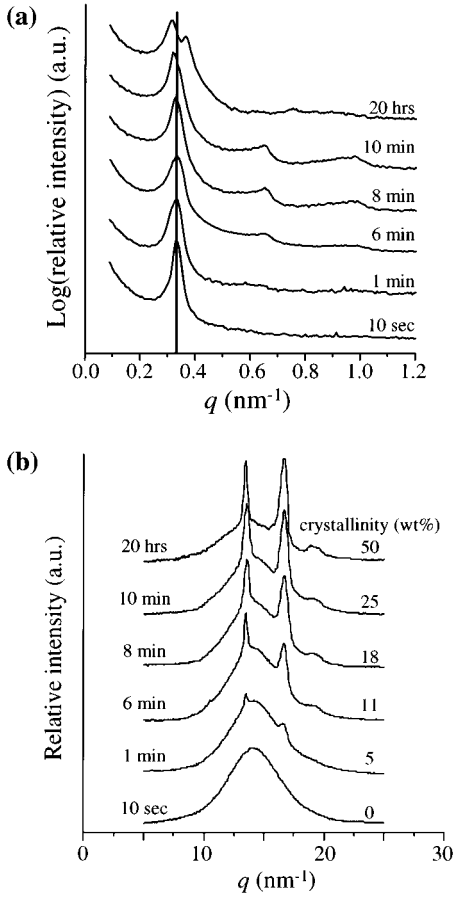

Figure 6. Azimuthal integrated SAXS (a, top) and WAXS (b, bottom) curves (from Figure 5) at different crystallization times.

The azimuthal integrated SAXS results in Figure 6a show an interesting phenomenon. With increasing the t_c, the first-order scattering peak tends to shift to lower *q* values at t_c = 10 min and substantially broadens. This

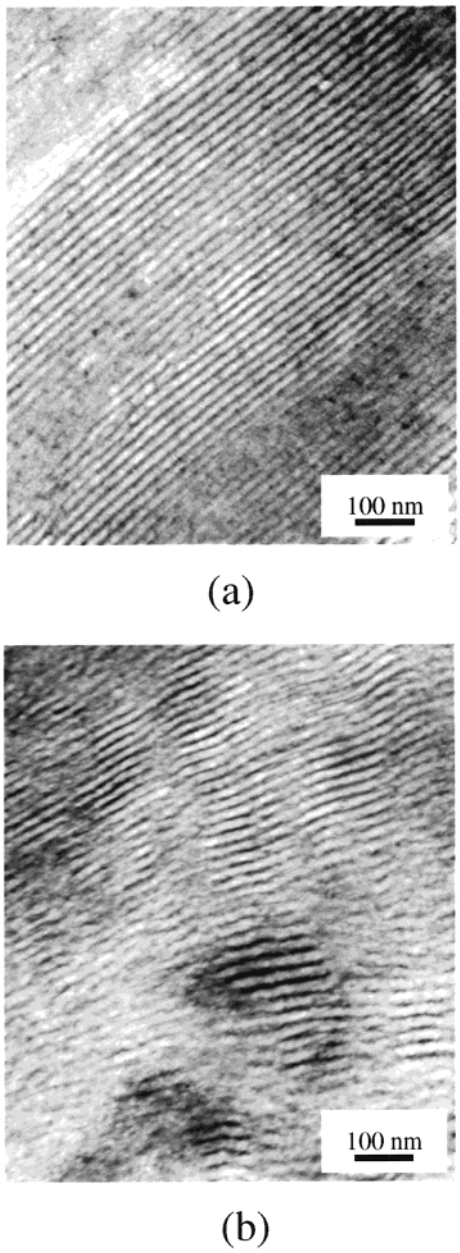

Figure 7. TEM micrographs of the PEO-*b*-PS sample: (a) after isothermally crystallized at 25 °C and (b) after self-seeded crystallized at 40 °C.

indicates that the PEO lamellar crystals can manipulate the phase morphology due to the fact that the PS glassy lamellae start to be weaken at 40 °C [close to the onset temperature (45 °C) of the PS T_g].[9] For t_c = 20 h, two diffraction peaks are observed at q = 0.31 nm^{-1} (20.0 nm) and q = 0.36 nm^{-1} (17.3 nm). Compared to the *d*-spacing in the melt of 18.7 nm, one *d*-spacing becomes greater and the other becomes smaller after self-seeded crystallization at 40 °C for a prolonged time. This is consistent with previous results that crystallization of the crystallizable blocks distorts the original phase morphology at temperatures close to the T_g of the amorphous blocks.[10] For low molecular weight PEO block copolymers, the PEO crystals may undergo both thickening and thinning processes (nonintegral folded to integral folded crystals) after self-seeded crystallization at relatively high temperatures.[29] Therefore, the *d*-spacing of 20.0 nm may be formed due to the PEO block crystal thickening, and the *d*-spacing of 17.3 nm

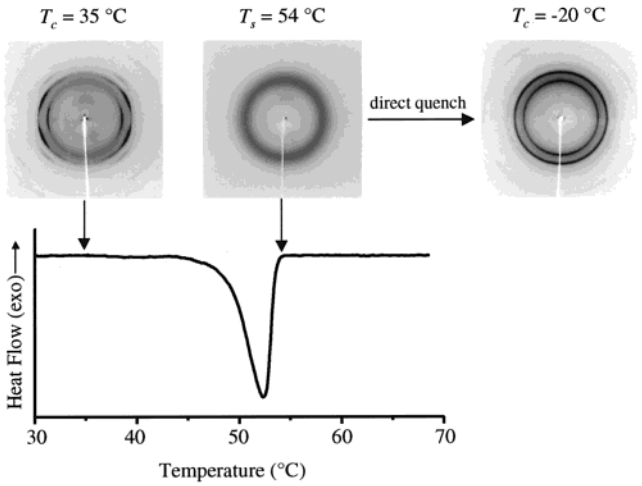

Figure 8. A self-seeding experiment on the shear-aligned PEO-*b*-PS represented by DSC and 2D WAXS. The sample was originally crystallized at 35 °C. After the self-seeding experiment, the sample was crystallized at −20 °C.

may be due to the PEO crystal thinning. The higher-order scattering feature in the SAXS pattern is somewhat lost at t_c = 20 h. This can also be visualized by the TEM observation as shown in Figure 7. Figure 7a shows the lamellar phase morphology after the sample is isothermally crystallized at 25 °C. A relatively uniform distribution of the lamellae can be found. Figure 7b is the phase morphology after self-seeded crystallization at 40 °C. The lamellar phase morphology in this figure shows less uniform thickness and orientation of the lamellae compared to that in Figure 7a. In particular, some areas exhibit thicker lamellar spacing than others. This may be associated with the formation of large grains of different lamellar thicknesses and "cross-talk" between neighboring lamellae. Detailed mechanisms are under further investigation.

To further support the observation that the crystal orientation is determined during the early stage of crystal growth, another self-seeded crystallization experiment is also designed. The shear-aligned sample is first crystallized at 35 °C, and a homeotropic crystal orientation is obtained as shown in the 2D WAXS along the *y* direction of Figure 8. The sample is then heated to a T_s = 54.0 °C at a slow rate of 1 °C/min. Similarly, the homeotropic crystal orientation in the sample does not lose until 54.0 °C is reached. From the DSC result shown in Figure 8, the residual crystallinity at 54.0 °C is less than 1 wt %. Subsequently, the sample is quickly quenched to −20 °C for isothermal crystallization. The crystallization rate at −20 °C is so fast that the crystallization process cannot be monitored using time-resolved simultaneous synchrotron 2D SAXS and WAXS experiments. The final crystal orientation after self-seeded crystallization at −20 °C detected by the 2D WAXS along the *y* direction (Figure 8), however, shows that most of the (120) reflection intensities are on the *z* direction, and minor intensities are in the *xy* plane. This indicates a homogeneous crystal orientation after the self-seeded crystallization at −20 °C.[1] Therefore, such a crystal orientation change in this self-seeding experiment also implies that the memory of the original homeotropic crystal orientation obtained at T_c = 35 °C is lost, although the self-seeds (primary nuclei) are generated from the homeotropically oriented crystals. It can thus be understood that the crystal orientation is not formed during the primary nucleation process but

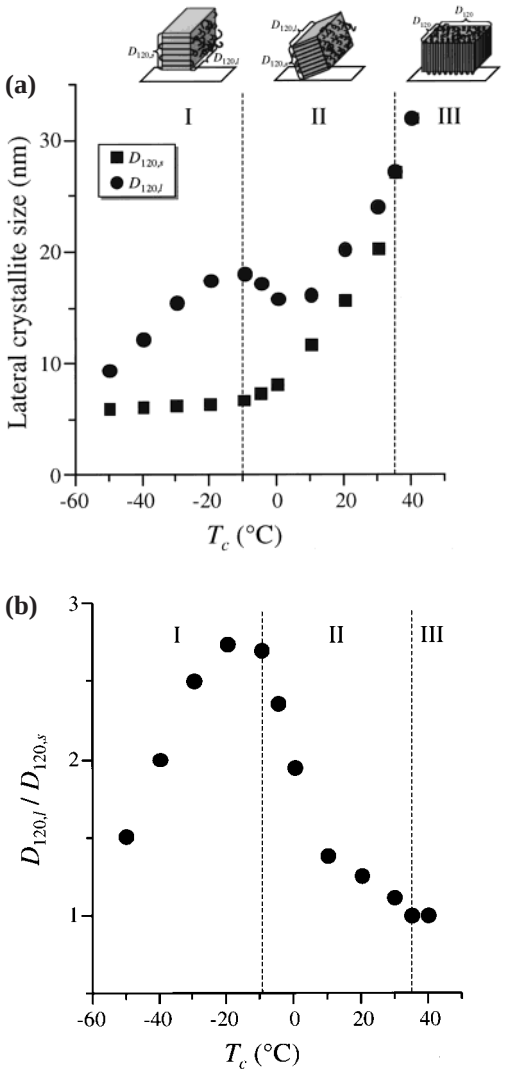

Figure 9. (a, top) Correlation length (apparent crystallite size) analyses for the (120) reflections in the 2D WAXS patterns along the *z* direction (see Figures 5, 9, and 14 in ref 1) at different T_c's. I, II, and III represent three temperature regions, respectively: I: $-50\ °C \le T_c \le -10\ °C$; II: $-5\ °C \le T_c \le 30\ °C$; III: $T_c \ge 35\ °C$. (b, bottom) The ratio of $D_{120,l}/D_{120,s}$ at different T_c's.

during the initial stage crystal growth. The poorer orientation of the WAXS reflection arcs in Figure 8 after crystallization at $T_c = -20\ °C$ (compared with that directly quenched from the melt at the same T_c in Figure 3b) may originate from the faster crystallization rate caused by the self-seeding process.

Apparent Crystallite Size Estimation Using the Scherrer Equation. To study the crystal growth dimension within the confined lamellae, we perform data analysis of the WAXS patterns along the *y* direction (Figures 5, 9, and 14 in ref 1) using the Scherrer equation to estimate the correlation length (apparent crystallite size) changes of the (120) reflections. As shown in Figure 9a, the correlation length of the (120) reflection along the *z* direction ($D_{120,s}$) is shorter than that in the *xy* plane ($D_{120,l}$) in the region of $-50\ °C \le T_c \le -10\ °C$. The crystal growth of PEO blocks in the *xy* plane is speculated to be less constrained than that along the *z* direction, because the crystal growth parallel to $\hat{n}$ is confined between two PS glassy lamellae. The crystal growth perpendicular to $\hat{n}$, on the other hand, is limited by an impingement of neighboring crystals, which is determined by the primary nucleation density. It should be noted that the calculated $D_{120,s}$, the correlation length parallel to $\hat{n}$, is around 6−7 nm, which may be a true crystal size since the spacing between two glassy PS lamellae is 8.8 nm. However, the calculated $D_{120,l}$, the correlation length perpendicular to $\hat{n}$, is merely a lower limit of actual crystal size in the *xy* plane, i.e., the $D_{120,l} \le$ actual crystal size in the *xy* plane. In this temperature region of $-50\ °C \le T_c \le -10\ °C$ (see Figure 9a), the $D_{120,s}$ keeps almost constant at 6−7 nm because of the 1D confinement along the *z* direction, while the $D_{120,l}$ gradually increases with increase the T_c because of continuous perfection of the crystals and a decrease of the primary nucleation density with increasing the T_c. On the other hand, an extrapolation shows that at $T_c = -60\ °C$ $D_{120,s} = D_{120,l}$, indicating an isotropic correlation length of the crystals when $T_c \le -60\ °C$.

When T_c changes from −5 to 30 °C, the *c* axis orientation starts to tilt from the *xy* plane. One can also see that there are two correlation lengths of the (120) reflections (see Figure 9 in ref 1). One is parallel to the *xy* plane (i.e., $D_{120,l}$), in which the (120) growth direction is perpendicular to $\hat{n}$, and the other is the (120) growth direction that is tilted with respect to $\hat{n}$ (i.e., $D_{120,s}$). Below $T_c = 0\ °C$, there is only a slight increase in $D_{120,s}$. Note that at $T_c = 0\ °C$ the tilt angle of the *c* axis away from the *xy* plane is 45°.[1] It is evident that only when the tilt angle exceeds 45° ($T_c > 0\ °C$) can the $D_{120,s}$ substantially increase (Figure 9a), indicating a gradual release of the 1D confinement on $D_{120,s}$. At $T_c > 0\ °C$ the $D_{120,l}$ increases monotonically with increasing T_c. On the other hand, there is a slight decrease in $D_{120,l}$ between $-10\ °C < T_c \le 0\ °C$. It is speculated that this kind of $D_{120,l}$ change between $-10\ °C < T_c \le 0\ °C$ may be associated with a change of nucleation mechanism from homogeneous to heterogeneous nucleation, since it was reported that the homogeneous to heterogeneous nucleation change for a PEO having a $\bar{M}_n$ of about 10K occurred at a T_c around 0 °C.[30] However, detailed investigation is necessary to obtain a quantitative understanding. With further increasing the T_c (>10 °C), the difference between these two $D_{120,l}$ and $D_{120,s}$ decreases, indicating a decrease in the anisotropic growth along both (120) directions. Finally, the $D_{120,s}$ and $D_{120,l}$ become identical above $T_c = 35\ °C$, revealing an isotropic growth along both of the (120) direction in the confined lamellae.

If we plot the ratio of $D_{120,l}/D_{120,s}$ vs T_c, the result illustrates the anisotropic crystal growth along both of the (120) directions, as shown in Figure 9b. Between $-50\ °C \le T_c \le -10\ °C$, $D_{120,l}/D_{120,s}$ slightly increases from 2.1 to 2.7, indicating a 1D crystal growth in the confined lamellae, and the anisotropy of the 1D crystal growth increases with increasing T_c. This is most likely due to a decrease of the primary nucleation density, since along the $D_{120,l}$ direction confinement is provided by the impingement of neighboring crystals. Between $-5\ °C \le T_c \le 30\ °C$, $D_{120,l}/D_{120,s}$ decreases from 2.4 toward 1.0, indicating that the crystal growth dimensionality changes from 1D toward 2D. Finally, above $T_c = 35\ °C$, $D_{120,l}/D_{120,s}$ becomes unity, revealing a 2D isotropic crystal growth in the confined lamellae. Therefore, different crystal orientations in different T_c regions are closely related to different crystal growth dimensionality in the 1D confined lamellae. When the nucleation density is extremely high, as in the case of $T_c <$

−50 °C, little crystal growth is necessary for crystallization (almost zero-dimension crystal growth). The crystal orientation is random in the 1D confined space. As the nucleation density gradually decreases as the T_c is raised to $-50\ °C \leq T_c \leq -10\ °C$, the crystal growth becomes 1D, and the crystal orientation is homogeneous in the 1D-confined space. With further decreasing the nucleation density in the temperature reign of $-5\ °C \leq T_c \leq 30\ °C$, the crystal growth changes from 1D toward 2D, and the crystal orientation is tilted from the lamellar surface. Finally, as the nucleation density is very low when $T_c \geq 35\ °C$, the crystal growth becomes 2D, and the crystal orientation is homeotropic in the confined lamellae.

Conclusion

The crystal (the *c* axis) orientation changes in a shear-aligned PEO-*b*-PS diblock copolymer within a nanoconfined lamellar environment have been found to be dependent only upon the T_c.[1] Using time-resolved simultaneous 2D SAXS and WAXS experiments, the crystal orientation is determined to occur in the early stage of crystallization which possess a crystallinity of <5 wt %. On the basis of specifically designed self-seeding experiments, we can further confirm that the crystal orientation in these confined lamellae is not determined by the primary nucleation but dominated by the initial step of crystal growth. The crystal growth dimension undergoes a gradual evolution from a 1D to a 2D. This can be evidenced by changes of the (120) correlation lengths along two perpendicular directions within the confined lamellar spaces. It is speculated that only when the crystal sizes are large enough can they feel the restriction of the confined lamellae, and therefore, the crystal orientation is determined in correspondence with different crystal growth dimensionalities.

Acknowledgment. This work was supported by NSF (DMR-9617030). The simultaneous SAXS and WAXS experiments were carried out at Beamline X27C at the National Synchrotron Light Source in Brookhaven National Laboratory (supported by Department of Energy).

References and Notes

(1) Zhu, L.; Cheng, S. Z. D.; Calhoun, B. H.; Ge, Q.; Quirk, R. P.; Thomas, E. L.; Hsiao, B. S.; Yeh, F.; Lotz, B. *J. Am. Chem. Soc.* **2000**, *122*, 5957.
(2) Giannelis, E. P.; Krishnamoorti, R.; Manias, E. *Adv. Polym. Sci.* **1999**, *138*, 107.
(3) Park, J.-Y.; McKenna, G. B. *Phys. Rev. B* **2000**, *61*, 6667.
(4) Jiang, C. H.; Zhang, G. L.; Zhang, H. Z.; Qi, Z. N. *Acta Polym. Sin.* **1999**, *6*, 765.
(5) Ogata, N.; Kawakage, S.; Ogihara, T. *Polymer* **1997**, *38*, 5115.
(6) Bates, F. S.; Fredrickson, G. H. *Annu. Rev. Phys. Chem.* **1990**, *41*, 525.
(7) Weimann, P. A.; Hajduk, D. A.; Chu, C.; Chaffin, K. A.; Brodil, J. C.; Bates, F. S. *J. Polym. Sci., Polym. Phys.* **1999**, *37*, 2053.
(8) Loo, Y.-L.; Register, R. A.; Ryan, A. J. *Phys. Rev. Lett.* **2000**, *84*, 4120.
(9) Zhu, L.; Cheng, S. Z. D.; Calhoun, B. H.; Ge, Q.; Quirk, R. P.; Thomas, E. L.; Hsiao, B. S.; Yeh, F.; Lotz, B. *Polymer*, in press.
(10) Zhu, L.; Chen, Y.; Zhang, A.; Calhoun, B. H.; Chun, M.; Quirk, R. P.; Cheng, S. Z. D.; Hsiao, B. S.; Yeh, F.; Hashimoto, T. *Phys. Rev. B* **1999**, *60*, 10022.
(11) Lotz, B.; Kovacs, A. J. *Kolloid Z. Z. Polym.* **1966**, *209*, 97.
(12) Lotz, B.; Kovacs, A. J.; Bassett, G. A.; Keller, A. *Kolloid Z. Z. Polym.* **1966**, *209*, 115.
(13) Kovacs, A. J.; Lotz, B.; Keller, A. *J. Macromol. Sci. Phys.* **1969**, *B3* (3), 385.
(14) Hirata, E.; Ijitsu, T.; Hashimoto, T.; Kawai, H. *Polymer* **1975**, *16*, 249.
(15) Yang, Y.-W.; Tanodekaew, S.; Mai, S.-M.; Booth, C.; Ryan, A. J.; Bras, W.; Viras, K. *Macromolecules* **1995**, *28*, 6029.
(16) Douzinas, K. C.; Cohen, R. E. *Macromolecules* **1992**, *25*, 5030.
(17) Cohen, R. E.; Bellare, A.; Drzewinski, M. A. *Macromolecules* **1994**, *27*, 2321.
(18) Séguéla, R.; Prud'homme, J. *Polymer* **1989**, *30*, 1446.
(19) Hamley, I. W.; Fairclough, J. P. A.; Ryan, A. J.; Bates, F. S.; Towns-Andrews, E. *Polymer* **1996**, *37*, 4425.
(20) Hamley, I. W.; Fairclough, J. P. A.; Terrill, N. J.; Ryan, A. J.; Lipic, P. M.; Bates, F. S.; Towns-Andrews, E. *Macromolecules* **1996**, *29*, 8835.
(21) Hamley, I. W.; Wallwork, M. L.; Smith, D. A.; Fairclough, J. P. A.; Ryan, A. J.; Mai, S.-M.; Yang, Y. W.; Booth, C. *Polymer* **1998**, *39*, 3321.
(22) Hillmyer, M. A.; Bates, F. S. *Macromol. Symp.* **1997**, *117*, 121.
(23) Zhu, L. Ph.D. Dissertation, Department of Polymer Science, The University of Akron, Akron, OH 44325-3909, 2000.
(24) Quirk, R. P.; Kim, J.; Kausch, C.; Chun, M. S. *Polym. Int.* **1996**, *39*, 3.
(25) Alexander, L. E. *X-ray Diffraction Methods in Polymer Science*; Wiley-Interscience: New York, 1969.
(26) Trent, J. S.; Scheinbeim, J. I.; Couchman, P. R. *Macromolecules* **1983**, *16*, 589.
(27) Kovacs, A. J.; Gonthier, A. *Colloid Polym. Sci.* **1972**, *250*, 530.
(28) Cheng, S. Z. D.; Chen, J.-H. *J. Polym. Sci., Polym. Phys. Ed.* **1991**, *29*, 311.
(29) Ryan, A. J.; Fairclough, J. P. A.; Hamley, I. W.; Mai, S.-M.; Booth, C. *Macromolecules* **1997**, *30*, 1723.
(30) Koutsky, J. A.; Walton, A. G.; Baer, E. *J. Appl. Phys.* **1967**, *38*, 1832.

MA001882P